

Fractalized magnon transport on a quasicrystal with enhanced stabilityJunmo Jeon¹,* Se Kwon Kim¹,† and SungBin Lee¹,‡*Korea Advanced Institute of Science and Technology, Daejeon 34141, South Korea* (Received 12 August 2022; revised 26 September 2022; accepted 10 October 2022; published 25 October 2022)

Magnonics has been receiving significant attention in magnetism and spintronics because of its premise for devices using spin current carried by magnons, the quanta of spin-wave excitations of macroscopically ordered magnetic media. Although magnonics has a clear energywise advantage over conventional electronics due to the absence of Joule heating, inherent magnon-magnon interactions give rise to a finite lifetime of magnons, which has been hampering the efficient realization of magnonic devices. To promote magnonics, it is imperative to identify the delocalized magnon modes that are minimally affected by magnon-magnon interactions and thus possess a long lifetime and use them to achieve efficient magnon transport. Here, we suggest that quasicrystals may offer the solution to this problem via critical magnon modes that are neither extended nor localized. We find that a critical magnon exhibits fractal characteristics that are absent in conventional magnon modes in regular solids such as a unique power-law scaling and a self-similar distribution of distances showing perfect magnon transmission. Moreover, critical magnons have longer lifetimes compared to the extended ones in a periodic system, by suppressing the magnon-magnon interaction decay rate. Such an enhancement of the magnon stability originates from the presence of the quasiperiodicity and intermediate localization behavior of critical magnons. Thus, we offer the utility of quasicrystals and their critical spin-wave functions in magnonics as unique fractal transport characteristics and enhanced stability.

DOI: [10.1103/PhysRevB.106.134431](https://doi.org/10.1103/PhysRevB.106.134431)**I. INTRODUCTION**

Magnonics is an emerging field in magnetism that concerns various applications of magnons, the quanta of spin-wave excitations of ordered magnets, in storing, transporting, and processing information [1–4]. Unlike traditional electronics where the information is carried by electric charges and thus the corresponding information transport generally gives rise to a finite-energy dissipation through Joule heating, magnonics are free from such Ohmic dissipation since the information is carried by magnons that are electrically neutral [5,6]. Because of this practical benefit, magnon transport has been gaining extensive interest from researchers in magnetism [7,8]. Despite such advantages, however, it is still a challenge to improve their lifetime and diffusion length scale [9–11]. Typically, magnons have a finite lifetime of about ns to μ s, which is mainly governed by magnon-magnon interactions, magnon-phonon interactions, disorder effects, and, in itinerant magnets, magnon-electron interactions [12–15]. A long lifetime is generally required to achieve long-distance spin transport, a high-quality factor of magnetic resonators, and also to integrate magnons in quantum information technology [16,17]. Hence, enhancing the lifetime of magnons is a crucial step to advance magnonics with potential applications [17].

To enhance the lifetime of magnons, it is imperative to establish new magnon characteristics distinct from conven-

tional ones. Here, as a strategy, we suggest a unique solid-state device made of magnetic quasicrystals and discuss their magnonic behavior. Unlike ordinary periodic systems having a unit length scale, quasicrystals refer to ordered but not periodic systems [18,19]. Due to the absence of a periodic length scale, the magnon exhibits distinct wave functions resulting in anomalous transport [20–25]. More specifically, in a conventional periodic system, there are two different types of wave functions; extended and localized states. First, a localized wave function would not decay in the presence of a perturbative interaction. This is because it exponentially decays in space, and hence the opportunity to interact with other states becomes negligible [1–3,26]. However, a localized wave function cannot be used in transport [27]. On the other hand, extended states contribute to transport but they could widely experience a decay process by magnon-magnon interactions. Hence, there is the dilemma of choosing an extended magnon or localized magnon for efficient spin transport. To circumvent this dilemma in conventional magnetic crystals, we suggest magnetic quasicrystals and their unique quantum states originating from exotic quasiperiodic ordering, which are known as critical states, as alternative spin carriers with an enhanced lifetime. Importantly, unlike conventional crystals, quasicrystals can admit a unique eigenstate, a so-called critical state described as neither extended nor localized but power-law decaying with a nontrivial fractal structure [28,29]. Thus, one may expect that such a critical magnon state can be used to transport with an enhanced lifetime as compared to ordinary extended magnons.

In this paper, we provide unique fractal spin-wave transport characteristics and lifetime enhancement under

*junmo1996@kaist.ac.kr

†sekwonkim@kaist.ac.kr

‡sungbin@kaist.ac.kr

quasiperiodically arranged magnetic media. We employ a Fibonacci quasicrystal as the magnetic media whose quasiperiodicity is encoded in the ratio of two different ferromagnetic XY exchange interactions, which we denote by J_A and J_B [30–34]. We analytically obtain spin-wave transmittance in the quasicrystal and clarify its nontrivial fractal characteristics. It turns out that critical spin transport exhibits a power-law decaying behavior, whose power could be controllable in terms of the strength of the quasiperiodicity. Surprisingly, a perfect spin-wave transmittance occurs at a certain set of length scales, which by themselves exhibit self-similarity. Furthermore, we show that the decay rates of the critical magnons are largely suppressed compared to the case of extended magnons in a periodic limit and this results in an enhancement of the magnon lifetime. Our work shows that the critical magnons of the quasicrystals could be a candidate for a stable magnetic information carrier in magnonics.

II. FRACTAL SPIN WAVE AND ANOMALOUS TRANSPORT

Let us consider the ferromagnetic XY spin chain of a quasicrystal under a strong magnetic field along the z direction, h . The Hamiltonian is given by

$$\mathcal{H} = \frac{1}{2} \sum_{i=1}^{N-1} J_{i,i+1} (S_i^+ S_{i+1}^- + S_{i+1}^+ S_i^-) + h \sum_{i=1}^N S_i^z, \quad (1)$$

where $J_{i,i+1}$, the exchange interaction between spins at the i th site and the $(i+1)$ th site, is arranged quasiperiodically (see the green region in Fig. 1) [30–32]. The total number of sites is N and S_i^{\pm} is the spin raising/lowering operator at the i th site.

Before discussing anomalous spin-wave transport in a ferromagnetic quasicrystalline magnet, we first characterize the spectrum within the linearized spin-wave theory. Note that the Holstein-Primakoff (HP) transformations map the spin operators to the bosonic operators $\hat{b}_i, \hat{b}_i^\dagger$ as $S_i^+ = \sqrt{2S - m_i} \hat{b}_i, S_i^- = \hat{b}_i^\dagger \sqrt{2S - m_i}, S_i^z = S - \hat{m}_i$ with the magnon number operator $m_i = \hat{b}_i^\dagger \hat{b}_i$ [35]. After the HP transformation, the leading term of Eq. (1) is equivalent to the tight-binding model of bosons with a uniform potential energy $h(NS - 1)$ per site that has a sublattice symmetry. In detail, the quadratic Hamiltonian H_2 is given by

$$H_2 = \frac{S}{2} \sum_{i=1}^{N-1} (\hat{b}_i^\dagger J_{i,i+1} \hat{b}_{i+1} + \text{H.c.}) + h \sum_{i=1}^N (S - m_i). \quad (2)$$

Here, the sublattice symmetry is given by sets of even and odd sites since we take into account the nearest-neighbor interaction only. Thus, the magnon dispersion should be symmetric in energy with respect to the uniform potential energy [27]. Throughout the paper, we consider odd N cases, where the energy $h(NS - 1)$ is exactly in the middle of the spectrum, and thus we term it as the middle energy.

The middle-energy magnon mode could be more relevant in magnon-based spin transport than low-energy magnon modes for the following reason. Note that to implement efficient spin-wave transport, we need a sufficiently large group velocity of the magnon mode [36]. However, the low-energy magnon modes generally have small group velocities

compared to the middle-energy magnon mode. Thus, in this work, we consider the transport characteristics of middle-energy magnons, which can be probed by nonlocal spin-wave spectroscopy experiments as demonstrated in Refs. [37–39]. Nevertheless, in a Fibonacci quasicrystal [40], the low-energy magnon modes, especially the ground state, have similar localization characteristics such as a self-similar structure and a power-law decaying which we will discuss. Hence, our results could be also applicable for low-energy magnon modes. See Appendix C for detailed information about the lowest-energy magnon mode.

The middle-energy magnon mode is exactly solvable as follows [29]. For a magnon mode with the energy given by $\hbar(NS - 1)$, the Schrödinger equation is written as $J_{i+1,i+2}\psi(i+2) + J_{i,i+1}\psi(i) = 0$, where $\psi(x) = \langle \Omega | \hat{b}_x | \psi \rangle$ represents the middle-energy magnon mode $|\psi\rangle$ and $|\Omega\rangle$ is the magnon vacuum. Thus, the middle magnon state is generally written as

$$\psi(2i+1) = \psi(1) \prod_{k=1}^i \left(-\frac{J_{2k-1,2k}}{J_{2k,2k+1}} \right). \quad (3)$$

For a periodic limit where $J_{i,i+1} = J$, the state is uniform, and hence represents an extended state. If two exchange coefficients J_A and J_B are periodically alternating such as in an “ABABAB” manner, then the product in Eq. (3) blows up or collapses as n increases for $J_A > J_B$ or $J_A < J_B$, respectively. Thus, the middle-energy magnon is localized at either $i = 1$ or $i = N$, respectively. Note that such a localization mode is equivalent to the zero-energy mode of the Su-Shrieffer-Heeger model [41].

On the other hand, in quasicrystals where J_A and J_B are quasiperiodically arranged, the spatial distribution of the middle-energy magnon mode exhibits a nontrivial fractal structure [28,29]. In detail, let $\kappa = \log \rho$ with $\rho = J_A/J_B$ be the strength of the quasiperiodicity. For the pattern-dependent function a defined by $a(AB) = 1, a(BA) = -1$, and $a(AA) = a(BB) = 0$ for the local patterns AB, BA, AA , and BB , the wave function on the $(2n+1)$ th site is given by

$$\psi(2n+1) = (-1)^n \psi(1) e^{\kappa H(n)}. \quad (4)$$

Here, $H(n)$ is known as the height field given by $H(n) = \sum_{i=1}^{2n-1} a(w_{[2i-1,2i+1]})$, where $w_{[x,y]}$ is the local pattern from site x to site y [29]. $H(n)$ is pattern dependent, thus, the middle state given by Eq. (4) is also pattern dependent whose dependency is controlled by the strength of the quasiperiodicity, κ . Moreover, the transmittance is invariant under the exchange of A, B links which would be encoded by $\kappa \rightarrow -\kappa$ and $H(n) \rightarrow -H(n)$. Thus, the spin-wave function and the characteristics of magnon transport in a quasicrystal are solely determined by the variation of the height field.

For a concrete example, let us consider a Fibonacci quasicrystal where the quasiperiodic pattern resides in two distinct links A, B . In particular, a Fibonacci quasicrystal is generated by successive substitution maps $A \rightarrow AB$ and $B \rightarrow A$, thus giving rise to $A \rightarrow AB \rightarrow ABA \rightarrow ABAAB$, and so on [19,42]. The height field oscillates around zero in the Fibonacci quasicrystal (see Appendix B), and hence its mean value vanishes [24]. However, the variation of the height field would be nontrivial due to the quasiperiodicity of the

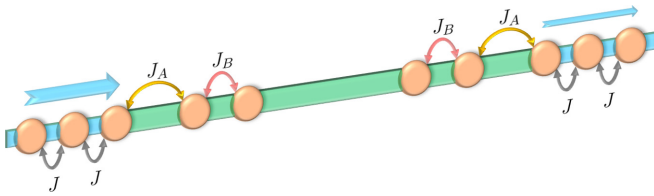


FIG. 1. The schematic experimental setup for spin-wave transport [Eq. (1)]. The two blue regions represent identical semi-infinite periodic leads with a uniform exchange magnitude J . The green region is the quasicrystal having quasiperiodically arranged exchanges J_A and J_B . Each red circle represents an identical magnetic atom. The direction and width of the blue arrows represent the direction of spin-wave transport and the amplitudes of spin waves at specific regions, respectively. For magnon transport, we generate a plane spin wave on the left infinity at the specific energy mode.

Fibonacci tiling pattern. Figure 2(a) illustrates the variation of the height field, $\text{Var}(H)(n) = \sum_{l \leq n} |H(l)|^2/n$. This shows that the variation of the height field $\text{Var}(H)(n)$ has the scaling behavior $\text{Var}(H)(n) \sim \log(n)$ [24,29]. Such logarithmic scaling behavior with self-similarity gives rise to the middle-energy critical state as shown in Fig. 2(b). In addition, the shape of the wave function is robust against small fluctuations on the J_A and J_B values. Thus, our following discussions about the unique spin-wave transport characteristics are applicable even for the case in the presence of a disorder effect. See Appendix D for detailed information.

A. Anomalous scaling of magnon transmittance

To discuss the unique spin-wave transport characteristics in magnetic quasicrystals, let us consider a setup where a quasicrystalline magnet is placed between two semi-infinite periodic spin chains as shown in Fig. 1. We generate a spin wave propagating from the left to the right as represented by the blue arrows in Fig. 1. As passing through the quasicrystal region (green region in Fig. 1), the amplitude of the spin wave would be changed.

From the Pichard formula, the transmittance is given in terms of the eigenvalues of the transfer matrix [43]. In par-

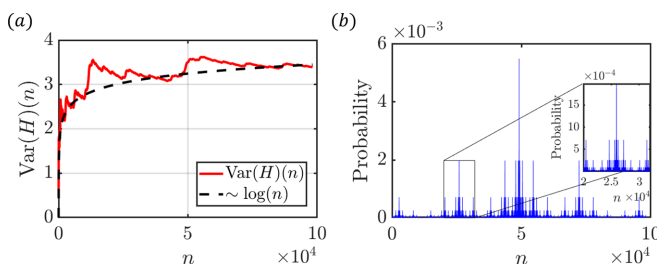


FIG. 2. (a) Logarithmic scaling behavior of the variation of a height field $\text{Var}(H)(n)$ given by $\sum_{l \leq n} |H(l)|^2/n$, where the argument n indicates the $(2n + 1)$ th site. (b) The spatial profile of the middle-energy state [Eq. (3)] which is the critical state having a power-law scaling and self-similar structures. The inset shows the self-similar structure of the spatial profile by zooming in from the 20 000th site to the 32 000th site region. Here, $\rho = J_A/J_B = 0.6$ and the system size $N = 196\,419$.

ticular, if we generate a middle-energy magnon plane wave from the left side, then the transmittance at the $(2n + 1)$ th site is given by [24,29]

$$T_{2n+1} = \text{sech}^2[\kappa H(n)]. \quad (5)$$

If $H(n)$ is a linear function, then the transmittance is exponentially decaying. For a zero height field in a periodic system, the transmittance becomes uniformly perfect. However, a nontrivial height field in quasicrystals leads to the unique characteristics of magnon transmittance.

First, since the typical $H(n)$ behaves as $\sqrt{\log(n)}$ in a Fibonacci quasicrystal, magnon transmittance decays much slower than the exponential decays. One can estimate the local dominant power $\alpha(n) \equiv -\log(T_{2n+1})/\log(2n)$ of the transmittance. It indicates the power-law decaying of the transmittance for the length of the system $2n$. By using Eq. (5), we note that $\alpha(n)$ is a decreasing function bounded by $0 \leq \alpha(n) \leq \kappa^2$. Hence, the most dominant decaying power $\alpha(n)$ is spatially dependent and upper bounded by the strength of the quasiperiodicity. Specifically, for stronger quasiperiodicity, the decaying power becomes larger and the transmittance decreases faster. Thus, the strength of quasiperiodicity controls the decay-rate power-law exponent of the transmittance.

B. Self-similar spin-wave transport signals

Now let us consider the case of a strong quasiperiodicity limit given by $\kappa \rightarrow \infty$. From Eq. (5), the transmittance vanishes except in the case of vanishing height field, $H(n) = 0$. Hence, the spin-wave signals appear only for these special sets of positions having a zero height field. The number of sites having a perfect transmittance grows as the system size increases (see Appendix B). Nevertheless, their distribution would exhibit a nontrivial fractality as the self-similar distribution of the height field. Figure 3 shows the transmittance distributions for a strong quasiperiodic limit. Interestingly, the positions showing perfect transmittance for any κ form a self-similar structure themselves. Specifically, the yellow regions in Fig. 3 exhibit a self-similar structure.

To quantify the fractality in the distribution of perfect transmittance, we compute its Hausdorff dimension [44]. Let q be the number of intervals whose length R is needed to cover the region where perfect transmittance appears. Then, the Hausdorff dimension is given by $D_F = -\frac{\partial(\log q)}{\partial(\log R)}$ [45]. The absence of fractality gives trivial Hausdorff dimensions, 0 or 1. On the other hand, the distribution of perfect transmittance gives a nontrivial Hausdorff dimension, $D_F \approx 0.9034$. Figure 3(d) illustrates the nontrivial Hausdorff dimension of the distribution of sites having perfect transmittance.

III. DECAY-RATE SUPPRESSION IN QUASICRYSTALS

For magnon applications, the stability of magnons with a long lifetime is one of the most important issues [1–3,17]. Generally, the magnon modes have a finite lifetime originating from various decaying process such as magnon-magnon or magnon-phonon interactions [12–15]. Particularly, we focus on how the magnon-magnon interaction affects the stability of the critical magnon mode in a Fibonacci quasicrystal. To explore the multimagnon interaction, the higher-order terms

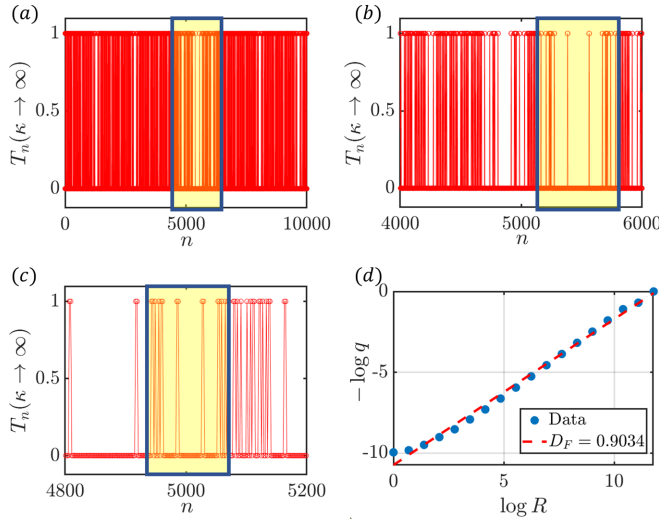


FIG. 3. Self-similar distribution of sites having perfect transmittance [Eq. (5)] in a Fibonacci quasicrystal in the limit of strong quasiperiodicity $\kappa \rightarrow \infty$, where the transmittance at a specific site has a value of either 0 or 1. Each panel shows n (a) from 0 to 10 000, (b) from 4000 to 6000, and (c) from 4800 to 5200 by zooming in five times. The yellow shaded regions exhibit a self-similar pattern of the distribution of perfect transmittance. (d) The nontrivial Hausdorff dimension $D_F = 0.9034$ indicates the presence of fractality of the distribution of sites having perfect transmittance in a Fibonacci quasicrystal. q is the number of intervals whose length R is needed to cover the region where perfect transmittance appears.

of HP transformations are considered [3,35]. At fourth order, the HP transformation of Eq. (1) gives rise to

$$H_4 = S \sum_{i=1}^{N-1} J_{i,i+1} \left(\frac{1}{4} \hat{b}_i^\dagger (m_i + m_{i+1}) \hat{b}_{i+1} + \text{H.c.} \right). \quad (6)$$

The Hamiltonian commutes with the total magnon number operator $\hat{N} = \sum_{i=1}^N m_i$, i.e., $[\mathcal{H}, \hat{N}] = 0$. Therefore, H_4 leads to the two-magnon interaction preserving the number of magnons in a ferromagnetic system.

From the Fermi's golden rule, the decay rate Γ originating from H_4 is given by

$$\Gamma_{i \rightarrow |f\rangle} = \frac{2\pi}{\hbar} \sum_f |\langle f | H_4 | i \rangle|^2 \rho_2(E_f). \quad (7)$$

Here, $\rho_2(E_f)$ is the two-particle density of states (DOS) for the total energy E_f . $|i\rangle$ and $|f\rangle$ are the initial and final states and their energies are the same, $E_f = E_i$. Such four-magnon scattering is important to understand the intrinsic damping of magnons for systems where the magnon number is conserved and therefore three-magnon scattering is absent [11,46].

Because of the energy conservation during the decay, if there is no $|f\rangle \neq |i\rangle$ state such that $E_f = E_i$, the decay rate in Eq. (7) vanishes. To avoid such trivial cases, we consider the case where the number of possible final states is maximized. Since a linearized bare Hamiltonian has sublattice symmetry, there are $(N+1)/2$ many particle-hole pairs of magnon modes whose energies are $E_\pm(\varepsilon) = h(NS-1) \pm \varepsilon$, and hence the total energy is the middle energy. Thus, in general, if we consider the two-particle sector of bosonic Fock

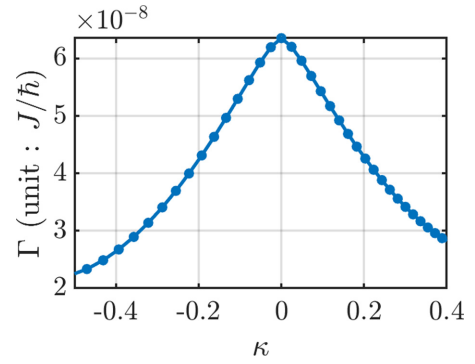


FIG. 4. Decay rate Γ as the function of the strength of the quasiperiodicity, κ . The strength of the quasiperiodicity increases as deviating from the periodic limit, $\kappa = 0$. As increasing the strength of the quasiperiodicity, the decay rate is suppressed. The initial and final states in the considered decaying processes are given by $|i\rangle = \frac{1}{\sqrt{2}} (\hat{b}_{E_0}^\dagger)^2 |\Omega\rangle$ and $|f\rangle = \hat{b}_{E_+}^\dagger \hat{b}_{E_-}^\dagger |0\rangle$ with $E_\pm \neq E_0$, where E_0 is the middle energy. The considered system size is $N = 10947$.

space, the middle-energy subspace has a maximal degeneracy with respect to the linearized bare Hamiltonian.

Let us consider the decay of two middle-energy magnon modes. The initial and final states are given by $|i\rangle = \frac{1}{\sqrt{2}} (\hat{b}_{E_0}^\dagger)^2 |\Omega\rangle$ and $|f\rangle = \hat{b}_{E_+}^\dagger \hat{b}_{E_-}^\dagger |0\rangle$ unless $E_\pm \neq E_0$, the middle energy. Here, $\hat{b}_\varepsilon^\dagger$ is the bosonic creation operator for an energy eigenstate with energy ε of the bare Hamiltonian. To capture the effect of the quasiperiodicity rather than the mere magnification of the interaction strength, we keep the total magnitude of the exchange interaction strength which appears directly in the decaying rate in Eq. (7). In detail, we keep $\sum_{i=1}^{N-1} J_{i,i+1}$ constant with $N-1$ the number of the links so that the average exchange interaction strength is J . When the numbers of A and B types of links are N_A and N_B , respectively, the proper J_A and J_B are $J_B = J(\rho N_A + N_B)^{-1}$ and $J_A = \rho J_B$ for a given strength of the quasiperiodicity, ρ [47].

On the other hand, the two-particle DOS at the total energy window $[E, E + dE]$ is given by $\rho_2(E) = \int_{E_{\min}}^{E_{\max}} \rho_1(\varepsilon) \rho_1(E - \varepsilon) d\varepsilon$, where $\rho_1(\varepsilon)$ is the one-particle DOS at the energy window $[\varepsilon, \varepsilon + d\varepsilon]$. In our case, $E = 2E_0$, where E_0 is the middle energy. For one-particle DOS, we use the local density of states (LDOS) which is given by $\text{LDOS}(i, \varepsilon) = -\sum_k \text{Im} \left(\frac{|V(i,k)|^2}{\varepsilon_k - \varepsilon + i0^+} \right)$. Here, the unitary matrix V is given by $H_2 = V D V^\dagger$ with the diagonal matrix D , $V(i, k)$ is the (i, k) element of the unitary matrix V , and ε_k is the energy of the k th energy level of H_2 . Then, the total single-particle DOS for the energy window $[\varepsilon, \varepsilon + d\varepsilon]$ is given by the spatial trace of LDOS.

Figure 4 shows how the decay rate changes in the presence of quasiperiodicity. As a function of quasiperiodicity κ , the decay rate Γ is suppressed. Here, the system size $N = 10947$ for each $\rho = J_A/J_B$. The decay rate Γ is maximized for a uniformly periodic limit where $J_A = J_B$. For the periodic limit, the initial states are both extended states, while for all other cases where $\rho \neq 1$, the initial states are both critical states. Since the critical states have an intermediate spatial distribution, neither extended nor localized, they also admit the intermediate decay rate between the extended and localized

states. Thus, the magnon decay rate of the critical state becomes smaller than the case of the extended state.

Note that the two-particle DOS, $\rho_2(E)$, also contributes to the decay rate. Since the quasiperiodicity makes the energy spectrum flatten and creates many gaps known as a fractal spectrum, the DOS would increase in quasicrystals [28]. Nevertheless, the decay rate is suppressed. Hence, we conclude that the magnons at the middle energy have a longer lifetime due to their fractal spatial distribution as critical states.

IV. DISCUSSION AND CONCLUSION

In conclusion, we have established self-similar spin-wave transport with enhanced stability in quasicrystals. Focusing on the critical magnon state at the middle of the spectrum, we have demonstrated that spin-wave transport is neither uniform nor exponentially decaying. Instead, it shows a power-law decaying behavior. In addition, we have shown that a magnetic quasicrystal can admit perfect transmittance at a special set of lengths. The distribution of such sites for perfect transmittance is independent on the strength of the quasiperiodicity, and exhibits a self-similar structure with a nontrivial Hausdorff dimension. Furthermore, we have shown that critical magnons are more stable under a magnon-magnon interaction compared to the conventional periodic case, resulting in a longer lifetime. Our findings suggest that the critical magnon states in magnetic quasicrystals may serve as long-lifetime spin carriers that are required to advance magnonics. The effects of other factors on the magnon lifetime such as magnon-phonon interactions and impurities in quasicrystals would be interesting future work.

Our work shows that magnetic quasicrystals can offer magnons with unusual characteristics that cannot be found in traditional magnetic crystals. It leads us to speculate that they might provide useful functionalities as well in current-driven spintronics, exhibiting, e.g., certain special forms of spin-transfer torque or spin-orbit torque that are hard to achieve with periodic magnetic systems [17,48–50]. More generally, we believe that magnetic quasicrystals would enrich the material library of magnonics and spintronics and thereby facilitate the advancement of both fields.

ACKNOWLEDGMENTS

J.M.J. and S.B.L. are supported by National Research Foundation Grants No. 2020R1A4A3079707 and No. 2021R1A2C1093060. S.K.K. was supported by Brain Pool Plus Program through the National Research Foundation of Korea funded by the Ministry of Science and ICT (NRF-2020H1D3A2A03099291).

APPENDIX A: HEIGHT FIELD AND ITS SIGNIFICANCE IN A PARTICLE-HOLE SYMMETRIC SYSTEM

In this Appendix, we introduce how the height field significantly characterizes the localization characteristics of the middle-energy state in a particle-hole symmetric system. Although we exemplify the two kinds of the links, say A and B , it can be generalized to a system involving more various types of links, say A , B , C , and so on. The height field

$H(n)$ for a system whose length is $2n$ is defined by $H(n) = \sum_{i=1}^{2n-1} a(w_{[2i-1,2i+1]})$, where $w_{[x,y]}$ is the local pattern from site x to site y . Here, a is the local pattern-dependent function defined by $a(AB) = 1$, $a(BA) = -1$, and $a(AA) = a(BB) = 0$ for the local patterns AB , BA , AA , and BB . Importantly, the height field is *not* a local quantity since it is summed over the whole tiling. Thus, the local changes do not change the characteristics of the height field. In terms of the tiling space topology, the height field is indeed the cohomological quantity of the pattern-equivariant topology. See Refs. [24,40] for detailed information on the topological robustness of the height field.

Let us consider a tight-binding model with nearest-neighbor (nn) hoppings which has sublattice symmetry or particle-hole symmetry. The sublattice is given by a set of odd sites (say α) and even sites (say β). Then, the Hamiltonian H_{nn} would be written as $H_{\text{nn}} = \sum_{i \in \alpha, j \in \beta, \langle i, j \rangle} t_{ij} (c_i^\dagger c_j + \text{H.c.})$ and the sublattice symmetry operator Ξ is given by $\Xi = \sum_{i \in \alpha} c_i^\dagger c_i - \sum_{j \in \beta} c_j^\dagger c_j$, where c_i is the creation and annihilation operator at the i th site of either a fermionic or bosonic one. Here, $\langle i, j \rangle$ is a pair of nearest-neighboring sites. Note that $\Xi H_{\text{nn}} \Xi = -H_{\text{nn}}$, which indicates that if the energy E is in the spectrum of H_{nn} , then $-E$ is also in the spectrum.

Now let us consider the zero-energy or middle-energy state. From the Schrödinger equation for this energy, $H_{\text{nn}}\psi = 0$, we have the recursion relationship

$$t_{i+1,i+2}\psi(i+2) + t_{i,i+1}\psi(i) = 0, \quad (\text{A1})$$

where $\psi(i) = \langle \Omega | c_i | \psi \rangle$ is the zero-energy wave function. We solve the recursion relationship which results in a zero-energy wave function in terms of the height field. Specifically,

$$\psi(2n+1) = (-1)^n \psi(1) \rho^{H(n)}, \quad (\text{A2})$$

where $\rho = t_A/t_B$. Here, t_A and t_B are the hopping magnitudes for the A link and B link, respectively. Hence, the growing behavior of the height field determines the localization characteristics of the middle-energy mode in the particle-hole symmetric center. In the main text, we have already discussed the trivial examples for a uniformly periodic limit [$H(n) = 0$ or $\rho = 1$] and alternating periodic limit where $H(n)$ is linearly growing, thus the state is localized. As a nontrivial example where the height field grows logarithmically by oscillating around the zero, we have introduced the Fibonacci quasicrystal which is generated by the substitution maps $A \rightarrow AB$ and $B \rightarrow A$. In addition to these examples, we give two other nonperiodic cases: Silver-mean and the Cantor-set tilings. These tilings are generated by the substitution maps for two links A and B that are given by (silver-mean) $A \rightarrow AAB$ and $B \rightarrow A$ and (Cantor-set) $A \rightarrow ABA$ and $B \rightarrow BBB$. Figure 5 demonstrates that the characteristics of the height field are totally different in these two tilings. The silver-mean tiling shows a similar height field in the sense of oscillating around zero with a logarithmically growing variance, $\text{Var}(H)(n) \equiv \sum_{l < n} |H(l)|^2/n$. On the other hand, the Cantor-set tiling admits a monotonically growing height field which results in a localized state similar to the alternating periodic case. We also illustrate the resulting middle-energy eigenfunctions that are critical for silver-mean tiling and exponentially localized for Cantor-set tiling, respectively.

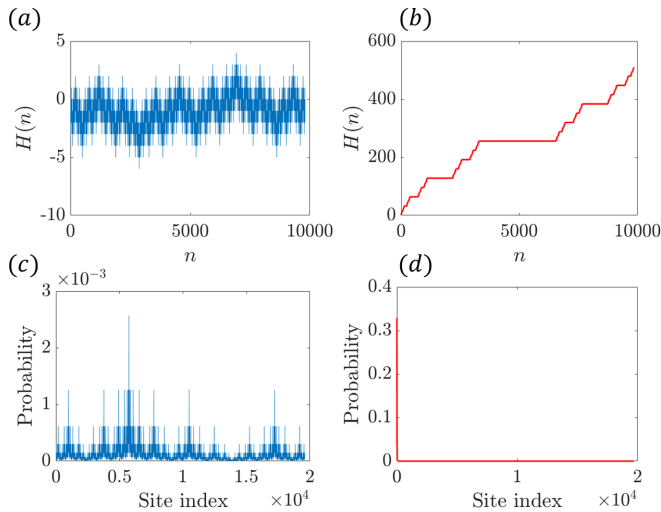


FIG. 5. The height field of (a) the silver-mean tiling and (b) Cantor-set tiling. The resulting middle-energy eigenstates given by Eq. (A2) are also illustrated in (c) the silver-mean tiling and (d) Cantor-set tiling as critically localized and exponentially localized, respectively. The strength of the quasiperiodicity, $\rho = t_A/t_B = 0.7$.

In such a way, the characteristics of the height field solely originating from the tiling pattern significantly determine the localization property of the middle-energy state.

APPENDIX B: OSCILLATING BEHAVIOR OF THE HEIGHT FIELD IN A FIBONACCI QUASICRYSTAL

In this Appendix, we briefly show that the average value of the height field in a Fibonacci quasicrystal vanishes. The Fibonacci quasicrystal is comprised of two letters A, B with the substitution maps $A \rightarrow AB, B \rightarrow A$. These substitution maps can be written in a matrix form $S = \begin{pmatrix} 1 & 1 \\ 1 & 0 \end{pmatrix}$. Since BB is forbidden under these substitution maps, there are only three types of length-2 supertiles in a Fibonacci quasicrystal, explicitly, $AA, AB,$ and BA . Let us denote them as $X, Y,$ and $Z,$ respectively. Now, let us renormalize the Fibonacci quasicrystal with these length-2 supertiles. For example, under this renormalization procedure, the first few parts of the Fibonacci quasicrystal $ABAABABA$ become $YXZZ$. Note that the pattern-dependent function a is given by $a(X) = 0, a(Y) = 1,$ and $a(Z) = -1$. Thus, the height field at site $n,$ $H(n),$ the cumulative sum of the function a up to the site $n,$ is given by $N_Y - N_Z$. Here, N_Y, N_Z are the number of Y and Z length-2 supertiles up to site n .

We claim that $N_Y - N_Z$ vanishes on average in the thermodynamic limit. To show this, we obtain the substitution maps for X, Y, Z supertiles induced by the original substitution maps for A, B tiles. By applying the original substitution maps three times for X, Y, Z supertiles, respectively, one can easily get the new substitution maps, $X \rightarrow YXZZY, Y \rightarrow YXZZ,$ and $Z \rightarrow YXZY$. These substitution maps for the supertiles

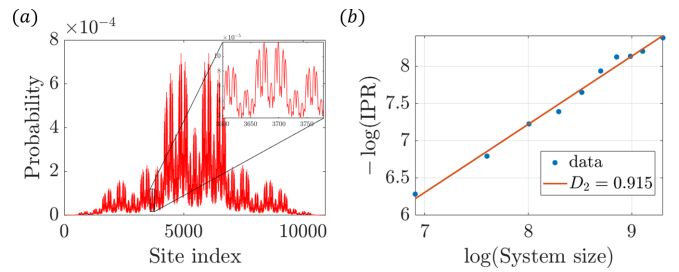


FIG. 6. Critical characteristics of the lowest-energy magnon mode. (a) The probability distribution of the lowest-energy magnon mode in space. The inset shows the self-similar structure of the critically localized lowest-energy magnon by zooming in from the 3600th site to the 3780th site. (b) Demonstration of the criticality of the lowest-energy magnon using the scaling of the inverse participation ratio (IPR). The criticality of the lowest-energy magnon mode is given by the fractal dimension $D_2 = 0.915$. The system sizes are tested up to $N = 10\,947, \rho = 0.7,$ and $J_A = 1$.

would be given by the matrix S' in Eq. (B1),

$$S' = \begin{pmatrix} 1 & 1 & 1 \\ 2 & 1 & 2 \\ 2 & 2 & 1 \end{pmatrix}. \quad (\text{B1})$$

Here, the basis is given by $N_X, N_Y, N_Z,$ the numbers of X, Y, Z supertiles in the tiling. The eigenvalues of the matrix S' are -1 and $2 \pm \sqrt{5}$. Especially, the eigenvalue -1 corresponds to the eigenvector $(0, 1, -1)^T$. This eigenvector corresponds to $N_Y - N_Z$. The eigenvalue -1 indicates that the quantity $N_Y - N_Z$ is oscillating, keeping its magnitude under the substitution map. Thus, in the thermodynamic limit, the mean value of the height field would be negligible on average as desired.

One of the interesting points is that there are infinitely many n in a zero-valued height field. Because the height field is oscillating around the zero on average, the pattern-dependent function a increases or decreases the height field by 1. Thus, at least one site between the oscillation of the height field takes a zero value. Hence, in the thermodynamic limit, we have infinitely many sites of the sites having a zero-valued height field which admit perfect transmittance regardless of the strength of the quasiperiodicity. See the main text for the unique self-similar distribution of these sites in a Fibonacci quasicrystal.

APPENDIX C: CRITICAL CHARACTERISTICS OF THE LOWEST-ENERGY MAGNON MODE

In this Appendix, we illustrate the critical characteristics of the lowest-energy magnon mode of a quadratic Holstein-Primakoff transformed Hamiltonian. Figure 6(a) shows the probability distribution of the ground state in space. The inset of Fig. 6(a) illustrates the self-similar structure of a lowest-energy magnon. Figure 6(b) quantifies this nontrivial criticality of the lowest-energy magnon in terms of the inverse participation ratio (IPR). The IPR of the wave function $\psi(i)$ is given by $\sum_i |\psi(i)|^4 / [\sum_i |\psi(i)|^2]^2$, where i is the site index. It is known that the IPR has scaling behavior as $\text{IPR} \sim N^{-D_2}$ for a sufficiently large system size N . The fractal dimension D_2 indicates the localization characteristics of the

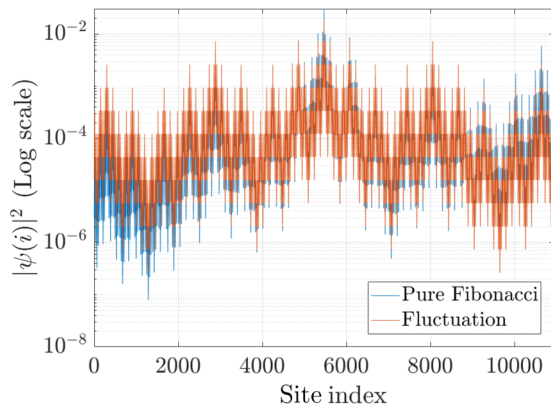


FIG. 7. Comparison of the probability distribution of the middle-energy state $|\psi(i)|^2$ in between the presence (orange) and the absence (blue) of the fluctuation on the interaction strengths J_A and J_B . Here, i is the site index. The level of the random fluctuation is 1% from the values of J_A and J_B in a pure Fibonacci chain without fluctuation. For the case of the absence of fluctuations, the strength of the quasiperiodicity is $\rho = 0.7$ and $J_A = 1$. Although a local wave function would be deformed under local fluctuations, the self-similar structure and the power-law behavior still appear.

wave function. In detail, $D_2 = 0$ for the exponentially localized state, $D_2 = 1$ for the extended state. For $0 < D_2 < 1$, we

can conclude that the wave function is fractal and critically localized with power-law behavior. Here, we find $D_2 = 0.915$ for the lowest-energy magnon mode [see Fig. 6(b)]. Such fractality originates from the structure of the Fibonacci chain. Hence, there are many other critically localized states.

APPENDIX D: CRITICALITY UNDER THE PRESENCE OF RANDOM FLUCTUATIONS ON INTERACTION STRENGTHS

Here, we discuss the critical properties such as the fractal structure and power-law behavior of the middle-energy state with respect to small random fluctuations on the spin-spin interaction strengths J_A and J_B . For given values of J_A and J_B , we add the 1% uniform random disorder effect. In detail, the spin-spin interaction magnitude of the A links and B links are given by $J_A + \eta_A$ and $J_B + \eta_B$, where $\eta_{A(B)} \in J_{A(B)}[-0.01, 0.01]$ is the uniform random disorder. Figure 7 compares the probability distribution of the middle-energy magnon modes for the cases of a pure Fibonacci chain (blue) and the presence of small fluctuations (orange). Even for a logarithmic scale, small disorder does not drastically change the wave function of the middle-energy magnon mode. Particularly, a self-similar structure and power-law behavior could be observed in both cases. Thus, the fractality of the transmittance and the power-law behavior of the magnon transport also appear even for the case of the presence of small fluctuations on the spin-spin interaction magnitude.

- [1] S. O. Demokritov, *Magnonics: From Fundamentals to Applications* (Springer, Berlin, 2013).
- [2] A. Prabhakar and D. D. Stancil, *Spin Waves: Theory and Applications*, Vol. 5 (Springer, Berlin, 2009).
- [3] S. M. Rezende, *Fundamentals of Magnonics* (Springer, Berlin, 2020), Vol. 969.
- [4] A. V. Chumak, V. I. Vasyuchka, A. A. Serga, and B. Hillebrands, Magnon spintronics, *Nat. Phys.* **11**, 453 (2015).
- [5] T. Schneider, A. A. Serga, B. Leven, B. Hillebrands, R. L. Stamps, and M. P. Kostylev, Realization of spin-wave logic gates, *Appl. Phys. Lett.* **92**, 022505 (2008).
- [6] A. Hirohata, K. Yamada, Y. Nakatani, I.-L. Prejbeanu, B. Diény, P. Pirro, and B. Hillebrands, Review on spintronics: Principles and device applications, *J. Magn. Magn. Mater.* **509**, 166711 (2020).
- [7] S. Takei and Y. Tserkovnyak, Superfluid Spin Transport Through Easy-Plane Ferromagnetic Insulators, *Phys. Rev. Lett.* **112**, 227201 (2014).
- [8] S. O. Demokritov, V. E. Demidov, O. Dzyapko, G. A. Melkov, A. A. Serga, B. Hillebrands, and A. N. Slavin, Bose-Einstein condensation of quasi-equilibrium magnons at room temperature under pumping, *Nature (London)* **443**, 430 (2006).
- [9] W. Yuan, Q. Zhu, T. Su, Y. Yao, W. Xing, Y. Chen, Y. Ma, X. Lin, J. Shi, R. Shindou *et al.*, Experimental signatures of spin superfluid ground state in canted antiferromagnet Cr_2O_3 via nonlocal spin transport, *Sci. Adv.* **4**, eaat1098 (2018).
- [10] L. Cornelissen, J. Liu, R. Duine, J. B. Youssef, and B. Van Wees, Long-distance transport of magnon spin information in a magnetic insulator at room temperature, *Nat. Phys.* **11**, 1022 (2015).
- [11] M. Sparks, *Ferromagnetic-Relaxation Theory* (McGraw-Hill, New York, 1964).
- [12] S. Streib, N. Vidal-Silva, K. Shen, and G. E. W. Bauer, Magnon-phonon interactions in magnetic insulators, *Phys. Rev. B* **99**, 184442 (2019).
- [13] A. Rückriegel, P. Kopietz, D. A. Bozhko, A. A. Serga, and B. Hillebrands, Magnetoelastic modes and lifetime of magnons in thin yttrium iron garnet films, *Phys. Rev. B* **89**, 184413 (2014).
- [14] Y. Hsu and L. Berger, Magnon heat conduction and magnon lifetimes in the metallic ferromagnet $\text{Fe}_{68}\text{Co}_{32}$ at low temperatures, *Phys. Rev. B* **14**, 4059 (1976).
- [15] A. L. Chernyshev, M. E. Zhitomirsky, N. Martin, and L.-P. Regnault, Lifetime of Gapped Excitations in a Collinear Quantum Antiferromagnet, *Phys. Rev. Lett.* **109**, 097201 (2012).
- [16] L. Trifunovic, F. L. Pedrocchi, and D. Loss, Long-Distance Entanglement of Spin Qubits via Ferromagnet, *Phys. Rev. X* **3**, 041023 (2013).
- [17] T. Chen, R. K. Dumas, A. Eklund, P. K. Muduli, A. Houshang, A. A. Awad, P. Dürrenfeld, B. G. Malm, A. Rusu, and J. Åkerman, Spin-torque and spin-Hall nano-oscillators, *Proc. IEEE* **104**, 1919 (2016).
- [18] D. Shechtman, I. Blech, D. Gratias, and J. W. Cahn, Metallic Phase with Long-Range Orientational Order and No Translational Symmetry, *Phys. Rev. Lett.* **53**, 1951 (1984).
- [19] J.-B. Suck, M. Schreiber, and P. Häussler, *Quasicrystals: An Introduction to Structure, Physical Properties and Applications* (Springer, Berlin, 2013), Vol. 55.
- [20] S. Roche, G. Trambly de Laissardière, and D. Mayou, Electronic transport properties of quasicrystals, *J. Math. Phys.* **38**, 1794 (1997).

- [21] D. Mayou, C. Berger, F. Cyrot-Lackmann, T. Klein, and P. Lanco, Evidence for Unconventional Electronic Transport in Quasicrystals, *Phys. Rev. Lett.* **70**, 3915 (1993).
- [22] Y. Xing, L. Qi, X. Zhao, Z. Lü, S. Liu, S. Zhang, and H.-F. Wang, Quantum transport in a one-dimensional quasicrystal with mobility edges, *Phys. Rev. A* **105**, 032443 (2022).
- [23] J. Bellissard, Anomalous transport: Results, conjectures and applications to quasicrystals, *Mater. Sci. Eng., A* **294**, 450 (2000).
- [24] J. Jeon and S. B. Lee, Topological critical states and anomalous electronic transmittance in one-dimensional quasicrystals, *Phys. Rev. Res.* **3**, 013168 (2021).
- [25] J. Jeon and S. Lee, Quantum bridge states and sub-dimensional transports in quasicrystals, [arXiv:2205.15343](https://arxiv.org/abs/2205.15343).
- [26] P. W. Anderson, *Basic Notions of Condensed Matter Physics* (CRC Press, Boca Raton, FL, 2018).
- [27] M. L. Cohen and S. G. Louie, *Fundamentals of Condensed Matter Physics* (Cambridge University Press, Cambridge, UK, 2016).
- [28] M. Kohmoto, B. Sutherland, and C. Tang, Critical wave functions and a Cantor-set spectrum of a one-dimensional quasicrystal model, *Phys. Rev. B* **35**, 1020 (1987).
- [29] N. Mace, A. Jagannathan, P. Kalugin, R. Mosseri, and F. Piechon, Critical eigenstates and their properties in one- and two-dimensional quasicrystals, *Phys. Rev. B* **96**, 045138 (2017).
- [30] X. Liu, Z. Du, and J.-M. Liu, Quantum fisher information for periodic and quasiperiodic anisotropic XY chains in a transverse field, *Quantum Inf. Process.* **15**, 1793 (2016).
- [31] D. Damanik, M. Lemm, M. Lukic, and W. Yessen, On anomalous Lieb–Robinson bounds for the Fibonacci XY chain, *J. Spectr. Theory* **6**, 601 (2016).
- [32] K. Hida, Renormalization group studies of the Fibonacci quantum spin chains, *J. Phys. Soc. Jpn.* **74**, 57 (2005).
- [33] S. Watanabe, V. S. Bhat, K. Baumgaertl, M. Hamdi, and D. Grundler, Direct observation of multiband transport in magnonic penrose quasicrystals via broadband and phase-resolved spectroscopy, *Sci. Adv.* **7**, eabg3771 (2021).
- [34] F. Lisiecki, J. Rychły, P. Kuświk, H. Głowiński, J. W. Kłos, F. Groß, N. Träger, I. Bykova, M. Weigand, M. Zelent, E. J. Goering, G. Schütz, M. Krawczyk, F. Stobiecki, J. Dubowik, and J. Gräfe, Magnons in a Quasicrystal: Propagation, Extinction, and Localization of Spin Waves in Fibonacci Structures, *Phys. Rev. Appl.* **11**, 054061 (2019).
- [35] T. Holstein and H. Primakoff, Field dependence of the intrinsic domain magnetization of a ferromagnet, *Phys. Rev.* **58**, 1098 (1940).
- [36] H. Qin, G.-J. Both, S. J. Hämäläinen, L. Yao, and S. van Dijken, Low-loss YIG-based magnonic crystals with large tunable bandgaps, *Nat. Commun.* **9**, 1 (2018).
- [37] V. Vlaminck and M. Bailleul, Current-induced spin-wave Doppler shift, *Science* **322**, 410 (2008).
- [38] O. Gladii, M. Haidar, Y. Henry, M. Kostylev, and M. Bailleul, Frequency nonreciprocity of surface spin wave in permalloy thin films, *Phys. Rev. B* **93**, 054430 (2016).
- [39] F. Ciubotaru, T. Devolder, M. Manfrini, C. Adelmann, and I. Radu, All electrical propagating spin wave spectroscopy with broadband wavevector capability, *Appl. Phys. Lett.* **109**, 012403 (2016).
- [40] J. Kellendonk, D. Lenz, and J. Savinien, *Mathematics of Aperiodic Order* (Springer, Berlin, 2015), Vol. 309.
- [41] W. P. Su, J. R. Schrieffer, and A. J. Heeger, Solitons in Polyacetylene, *Phys. Rev. Lett.* **42**, 1698 (1979).
- [42] C. H. O. Costa and M. S. Vasconcelos, Band gaps and transmission spectra in generalized Fibonacci $\sigma(p, q)$ one-dimensional magnonic quasicrystals, *J. Phys.: Condens. Matter* **25**, 286002 (2013).
- [43] P. A. Mello and J.-L. Pichard, Maximum-entropy approaches to quantum electronic transport, *Phys. Rev. B* **40**, 5276 (1989).
- [44] J. Rychły, J. W. Kłos, M. Mruczkiewicz, and M. Krawczyk, Spin waves in one-dimensional bicomponent magnonic quasicrystals, *Phys. Rev. B* **92**, 054414 (2015).
- [45] M. L. Lapidus, M. Van Frankenhuijsen, and B. B. Mandelbrot, *Fractal Geometry and Applications: A Jubilee of Benoît Mandelbrot* (American Mathematical Society, Providence, RI, 2004).
- [46] M. E. Zhitomirsky and A. L. Chernyshev, Colloquium: Spontaneous magnon decays, *Rev. Mod. Phys.* **85**, 219 (2013).
- [47] J. Jeon and S. B. Lee, Pattern-dependent proximity effect and Majorana edge mode in one-dimensional quasicrystals, *Phys. Rev. B* **105**, 064502 (2022).
- [48] I. Pallecchi, L. Pellegrino, A. Caviglia, E. Bellingeri, G. Canu, G. C. Gazzadi, A. S. Siri, and D. Marré, Current-driven hysteresis effects in manganite spintronics devices, *Phys. Rev. B* **74**, 014434 (2006).
- [49] A. Manchon and S. Zhang, Theory of spin torque due to spin-orbit coupling, *Phys. Rev. B* **79**, 094422 (2009).
- [50] J. Železný, P. Wadley, K. Olejník, A. Hoffmann, and H. Ohno, Spin transport and spin torque in antiferromagnetic devices, *Nat. Phys.* **14**, 220 (2018).